Journal of Hazardous Materials 159 (2008) 271–279

Contents lists available at ScienceDirect

Journal of Hazardous Materials

journal homepage: www.elsevier.com/locate/jhazmat

Geochemical modelling of arsenic and selenium leaching in alkaline water treatment sludge from the production of non-ferrous metals

Geert Cornelis[a,*], Sofie Poppe[b], Tom Van Gerven[a], Eric Van den Broeck[c], Michiel Ceulemans[d], Carlo Vandecasteele[a]

[a] *Laboratory of Applied Physical Chemistry and Environmental Technology, Department of Chemical Engineering, K.U. Leuven, W. De Croylaan 46, B-3001 Leuven, Belgium*
[b] *Total Refinery Antwerp, Scheldelaan 16, B-2030 Antwerpen, Belgium*
[c] *Umicore Cobalt and Specialty Materials, Watertorenstraat 33, B-2250 Olen, Belgium*
[d] *Umicore Precious Metals Refining, A. Greinerstraat 14, B-2660 Hoboken, Belgium*

ARTICLE INFO

Article history:
Received 25 July 2007
Received in revised form 2 February 2008
Accepted 12 February 2008
Available online 16 February 2008

Keywords:
Arsenic
Selenium
Modelling
Leaching
Precipitation
Adsorption
Solid solution

ABSTRACT

Geochemical modelling of leaching of oxyanion forming elements such as arsenic (As) and selenium (Se) is frequently not successful. A consistent thermodynamic dataset of As and Se was therefore composed, not only including precipitation, but also adsorption and solid solution, and was applied to the pH-dependent leaching behaviour of As and Se in an alkaline residue with a pH 11.1 from the lime treatment of sulphuric acid wastewaters from the production of non-ferrous metals. The As and Se content ranged up to 6.7 wt% and 0.29 wt%, respectively and speciation analysis showed that 96.3% of As occured as arsenate whereas Se speciation comprised 79% selenate and 21.0% selenite. XRD and SEM/EDX analysis showed that arsenate occurred as rauenthalite ($Ca_3(AsO_4)_2{\cdot}10H_2O$), associated with gypsum, the most important mineral. Arsenate and arsenite concentrations were only slightly below equilibrium with rauenthalite and calciumarsenite ($CaHAsO_3$), respectively and consideration of adsorption and solid solution only marginally improved model predictions. Selenate (Se^{VI}) and selenite (Se^{IV}), on the other hand, were far from equilibrium with their corresponding calcium metalate. The application of solid solutions and adsorption of Se^{VI} and Se^{IV} oxyanions with gypsum, calcite and ettringite significantly improved model predictions but missing thermodynamic data and especially the lack of a comprehensive model for solid solution and surface exchange with calcite and ettringite still hampered efficient modelling.

1. Introduction

Geochemical modelling is often used to understand and predict leaching of toxic contaminants in soils and sediments but, more recently, it has also been successfully applied to highly alkaline (pH > 11) waste products from industrial processes (e.g. [1–3]) to understand and control the leaching behaviour of heavy metals such as Cu, Pb and Zn. Modelling of oxyanion forming metal and metalloid elements such as As and Se, however, has been less successful because during leaching studies of alkaline wastes, these elements have received much less attention compared to other heavy metals such as Cu, Pb and Zn due to a frequently much lower total concentration [4–6]. The concentration found in waste leachates, on the other hand, can be high relative to their total content, because oxyanions are much more soluble in alkaline matrices compared to heavy metals [7]. Especially in realistic situations such as landfills, where the liquid-to-solid ratio is low, high concentrations can be found in porewaters. Because the knowledge still lacks how to reduce leaching, a better understanding of the geochemical fate of As and Se is needed because most chemical forms can cause adverse health effects and even death [8,9]. Moreover, the European Directive 1999/31/EC on landfilling of waste has recently been complemented by the Council Decision 2003/33/EC, establishing criteria and procedures for the acceptance of waste at landfills that include both As and Se [10].

Multiple redox states are possible in the case of As and Se and the predominating species in alkaline pore solutions, being arsenates ($H_xAs^{V}O_4^{x-3}$) and arsenites ($H_xAs^{III}O_3^{x-3}$) or selenates ($H_xSe^{VI}O_4^{x-2}$) and selenites ($H_xSe^{IV}O_3^{x-2}$) [7], are often thought to be in equilibrium with their corresponding calcium metalates in alkaline solid wastes, where calcium is the most important multivalent cation [2,11,12]. However, predictions based on calcium metalate precipitation usually fail for a number of reasons:

- Lack of knowledge of the redox state although this is crucial because calcium arsenites and calcium selenates are much more

* Corresponding author. Tel.: +32 16 322343; fax: +32 16 322991.
E-mail address: Geert.Cornelis@cit.kuleuven.be (G. Cornelis).

0304-3894/$ – see front matter © 2008 Elsevier B.V. All rights reserved.
doi:10.1016/j.jhazmat.2008.02.016

soluble compared to calcium arsenates and selenites, respectively [11,12].
- The use of inconsistent thermodynamic data that does not account for soluble aqueous complexes such as $CaAsO_4^-$, $CaHAsO_4$ or $CaH_2AsO_4^+$.
- The occurrence of other geochemical mechanisms such as adsorption and solid solution formation that are seldom taken into account.

In soils, surface complexation with iron and aluminium oxides usually is considered to be the dominant mechanism controlling oxyanion behaviour but in alkaline matrices, the surface of these oxides is predominantly negatively charged and adsorption of oxyanions thus is not favoured. Much progress has been made in the study of solid solution formation and adsorption of oxyanions to common minerals of alkaline matrices. It is, for example, well known that arsenate and selenate can be incorporated in ettringite ($Ca_6[Al(OH)_6]_2(SO_4)_3{\cdot}26H_2O$) [12,13], gypsum ($CaSO_4{\cdot}2H_2O$) [14,15]. Moreover, arsenite and selenate can be taken up in the structure of calcite ($CaCO_3$) [14,16–18], whereas selenite interacts with calcite and ettringite through surface exchange reactions [12,19,20]. This knowledge has, however, only rarely been applied in leaching studies and geochemical models (e.g. [2,21]).

The goal of the present study is to compose a consistent thermodynamic dataset for As and Se that can be used to model these elements in alkaline matrices and to investigate the importance of adsorption and solid solution, next to simple precipitation, in determining the leaching behaviour of As and Se. These models are then applied to an alkaline waste (pH > 11) resulting from the physicochemical treatment of wastewaters from the production of non-ferrous metals such as Se. The most common production processes, smelting or roasting of copper anode slime, generate highly acidic (0 < pH < 1.35) wastewaters rich in sulphuric acid [22] that contain considerable amounts of Se (up to 10 mg/l) and very high amounts of As (up to 2000 mg/l). Addition of lime and $FeCl_3$ to precipitate As is a common treatment procedure in case of these high As concentrations [23]. This sludge represents a relatively simple, though realistic, alkaline matrix composed of a limited amount of minerals. The only management option is landfilling because leaching of As and Se is very high and European standard leaching values for landfilling of hazardous wastes (25 mg/l for As and 7 mg/l for Se) regularly are not met, which not only invokes considerable costs, but also poses a severe threat to the environment. The production of the sludge is significant because the world's annual consumption of Se in 2004 was estimated at 2700 tonnes and is expected to have increased more recently, given the permanent high demands from China [24].

2. Experimental

2.1. Waste material

A sample of water treatment sludge from non-ferous metals production was obtained at an industrial site where it is produced by adding lime and $FeCl_3$ to the sulphuric acid wastewater. Lime is added until the suspension reaches a pH between 10.5 and 11.5. In a settling tank, the sludge is separated from solution and is brought to a moisture content of about 50% in a press after which it is stored open to the ambient atmosphere. Residence time of the sludge within the water treatment is only several hours.

2.2. Total content and leachability

Total elemental content was determined by digestion with concentrated HNO_3. Metal concentrations in the digest were determined with Inductively Coupled Plasma Mass Spectrometry (ICP-MS, Thermo X-series I). Leaching of metals was tested using the EN 12457-2 standard test: 10 g of dry material was agitated in 100 ml distilled water (liquid-to-solid ratio, L/S = 10) for 24 h. After filtration over a 0.45 μm membrane filter, element concentrations were measured with ICP-MS. In order to evaluate the pH dependence of metal leaching, a set of tests based on the EN-12457-2 standard test was used. Various volumes of concentrated HNO_3 or KOH 60% (w/w) were added to distilled water in order to obtain different leachate pH levels after 24 h on a flat-bed shaker. Metal and metalloid concentrations were determined in the filtrate with ICP-MS. Sulphate was quantified with ion chromatography (IC) (Dionex ICS-2000 with a 2-mm AS-18 column and KOH mobile phase gradient). Filtrates of a second pH-dependent leaching test were used to determine redox speciation of As and Se as a function of pH. The filtrates were diluted 1:1 with 0.1 M citrate in Nalgene cryo-vials that were stored in a freezer prior to speciation analysis. In these solutions, total As and Se concentration were determined with ICP-MS. As^{III} and Se^{IV} were quantified with Hydride Generation Inductively Coupled Optical Emission Spectroscopy (HG-ICP-OES) (Ciros CCP, SPECTRO Analytical Instruments) and As^{V} and Se^{VI} concentrations were calculated as the difference with total As and Se. Speciation of total As and Se (soluble + insoluble) was determined by agitating sludge samples at L/S = 200 and pH 1 for 24 h. In these conditions, all minerals were dissolved. As_{total} and Se_{total} in the extracts were again measured using ICP-MS. The extracted amounts of As and Se were equal to the total amount determined by digestion. The As^{V} and Se^{IV} concentrations were determined by quantifying AsO_4^{3-} and SeO_3^{2-} in the extracts using IC (AS-18 anion exchange column with a KOH mobile phase gradient) and As^{III} and Se^{VI} concentrations were then calculated as the differences As_{total}–As^{V} and Se_{total}–Se^{IV}.

Carbonate content was determined by adding 60 ml of distilled water and 40 ml of 5 M HCl to 5 g dry sludge. The formed CO_2 was stripped out using a flow of N_2-gas. This gas stream was led through two absorption bottles, each containing 50 ml of 1 M NaOH. After 2 h reaction time, the carbonate concentration in the absorption bottles was determined by titration with 0.5 M HCl.

2.3. Mineralogy

To reduce the gypsum content 5 g of the samples was washed for 24 h in 1 l water (L/S = 200) and the resulting sludge was filtrated and dried. Mineralogy of original and washed sludge samples was determined using X-ray diffraction (XRD) (Philips PW1130/90 Co Kα) with a 0.05° step size and 1 s acquisition time. Scanning electron microscopy (SEM) on the original samples in combination with energy dispersive spectrometry spot measurements (EDS) (Philips, XL 30 SEM FEG) provided additional information.

3. Modelling in PHREEQC

3.1. Model inputs

All model calculations were performed using the hydrogeochemical model PHREEQC, version 2.12.5.669 [25]. The leaching model for As and Se was evaluated by applying model calculations to pH-dependent leaching. Total amounts of Na, Mg, Al, Ca, Fe, Ba, As, Se, S, Si and CO_3^{2-} were used as model inputs. The Cl^- ion was not used as an input in the model but was used to compensate for charge imbalances. Other elements such as Zn and Pb were ignored because in preliminary model calculations it was observed that they did not have a significant effect on modelled results.

The total redox speciation of As and Se was estimated from the L/S = 200 at pH 1 extracts. Speciation of redox sensitive elements such as As, Se, Fe and S was made independent of the redox potential

Table 1
Thermodynamic data of soluble species of As and Se

Reaction	log *K*	Source
As^{V}		
$AsO_4^{3-} + H^+ = HAsO4^{2-}$	11.8	[34]
$HAsO_4^{2-} + H^+ = H_2AsO_4^-$	6.99	[34]
$H_2AsO_4^- + H^+ = H_3AsO_4^0$	2.30	[34]
$AsO_4^{3-} + Ca^{2+} = CaAsO_4^-$	6.22	[32]
	4.36	[33]
$HAsO_4^{2-} + Ca^{2+} = CaHAsO_4^0$	2.69	[32]
	2.66	[33]
$H_2AsO_4^- + Ca^{2+} = CaH_2AsO_4^+$	1.06	[32]
	1.30	[33]
$AsO_4^{3-} + Fe^{3+} = FeAsO_4^0$	18.9	[32]
$HAsO_4^{2-} + Fe^{3+} = FeHAsO_4^+$	6.45	[32]
$H_2AsO_4^- + Fe^{3+} = FeAsO_4^{2+}$	4.04	[32]
$AsO_4^{3-} + Fe^{2+} = FeAsO_4^-$	7.06	[32]
$HAsO_4^{2-} + Fe^{2+} = FeHAsO_4^0$	3.54	[32]
$H_2AsO_4^- + Fe^{2+} = FeAsO_4^+$	2.68	[32]
$AsO_4^{3-} + Al^{3+} = AlAsO_4^0$	18.9	[32]
$HAsO_4^{2-} + Al^{3+} = AlHAsO_4^+$	6.45	[32]
$H_2AsO_4^- + Al^{3+} = AlAsO_4^{2+}$	4.04	[32]
$AsO_4^{3-} + Mg^{2+} = MgAsO_4^-$	6.34	[32]
$HAsO_4^{2-} + Mg^{2+} = MgHAsO_4^0$	2.86	[32]
$H_2AsO_4^- + Mg^{2+} = MgH_2AsO_4^+$	1.52	[32]
As^{III}		
$AsO_3^{3-} + H^+ = HAsO3^{2-}$	15.00	[34]
$HAsO_3^{2-} + H^+ = H_2AsO_3^-$	14.10	[34]
$H_2AsO_3^- + H^+ = H_3AsO_3^0$	9.17	[34]
Se^{VI}		
$SeO_4^{2-} + H^+ = HSeO_4^-$	1.80	[52]
$HSeO_4^- + H^+ = H_2SeO_4$	−2.01	[52]
$SeO_4^{2-} + Ca^{2+} = CaSeO_4^0$	2.00	[52]
$SeO_4^{2-} + 2Na^+ = Na_2SeO_4^0$	0.02	[55]
$HSeO_4^- + Na^+ = NaHSeO_4^0$	0.01	[55]
$SeO_4^{2-} + Mg^{2+} = MgSeO_4^0$	2.2	[56]
Se^{IV}		
$SeO_3^{2-} + H^+ = HSeO_3^-$	8.54	[52]
$HSeO_3^- + H^+ = H_2SeO_3^0$	2.70	[52]
$SeO_3^{2-} + Ca^{2+} = CaSeO_3^0$	3.17	[57]

by disregarding all redox reactions during leaching given their slow kinetics [26,27]. All S was assumed to occur as sulphate. The Fe^{II}/Fe^{III} ratio was not experimentally determined but it was assumed that all soluble Fe at pH 8.4, where a minimum was observed in the pH-dependent leaching behaviour, was Fe^{II} because at that pH, the solubility of Fe^{II} is two orders of magnitude higher than the Fe^{III} solubility [28].

3.2. Aqueous speciation

The PHREEQC database was supplemented with data from the more extensive Visual Minteq v. 2.32 database [29] and the most recent thermodynamic data of hydrolysis and soluble complexes of As and Se-species available in the literature (Table 1). In case of the aqueous complexes $CaH_2AsO_4^+$, $CaHAsO_4^0$ and $CaAsO_4^-$, two datasets were found. Both datasets were independently used in two consecutive model calculations. A third model calculation was performed without these aqueous complexes because their existence is disputed by some authors [30,31]. The species in Table 1 were all obtained at or corrected to zero ionic strength.

3.2.1. Precipitation

Thermodynamic data of possible solids of As^{III}, Se^{VI} and Se^{IV} were taken from the literature (Table 2). Selection of possible As^{V} solids was largely based on mineralogical analysis as will be discussed further. Whenever solution composition data in equilibrium with the solids in Table 2 was available in the literature, solubility constants were recalculated according to the different aqueous

Table 2
Thermodynamic data of As and Se minerals

Reaction	log *K*	Source
As^{V}		
$FeAsO_4 = Fe^{3+} + AsO_4^{3-}$	−22.04	[58]
As^{III}		
$CaHAsO_3 = Ca^{2+} + HAsO_3^{2-}$	−10.4033	Calculated from [51]
$Ca(AsO_2)_2 + 2H_2O = Ca^{2+} + 2H_2AsO_3^-$	−6.5195	[51]
Se^{VI}		
$CaSeO_4{\cdot}2H_2O = Ca^{2+} + SeO_4^{2-} + 2H_2O$	−4.20	[59]
$Fe_2(SeO_4)_3 = 2Fe^{3+} + 3SeO_4^{2-}$	−23.19	[60]
$Ca_6Al_2(SeO_4)_3(OH)_{12}{\cdot}26H_2O + 12H^+ = 6Ca^{2+} + 2Al^{3+} + 3SeO_4^{2-} + 38H_2O$	73.40	[12]
Se^{IV}		
$CaSeO_3{\cdot}H_2O = Ca^{2+} + SeO_3^{2-} + H_2O$	−6.84	[12]
$Ca(HSeO_3)_2{\cdot}H_2O = Ca^{2+} + HSeO_3^- + H_2O$	−5.96	Calculated from [50]
$Fe_2(SeO_3)_3 = 2Fe^{3+} + 3SeO_3^{2-}$	−34.00	[61]

complexation and hydrolysis datasets of As and Se in Table 1 because other datasets were used in the references of Table 2 whilst calculating solubility products. In this way, a consistent thermodynamic database was obtained. Activity corrections were performed using the Davies Equation.

The solubility products of calcium arsenates were recalculated three times for three consecutive model attempts: one attempt assuming no soluble complexes, a second one assuming soluble complexes according to the dataset of Whiting [32] and a third attempt assuming soluble complexes according to Bothe and Brown [33]. Hydrolysis data of Nordstrom and Archer [34] were used at all times.

Solubility data for amorphous iron arsenate and selenite were implemented rather than their crystalline analogues given the short equilibration times during sludge production (several hours). A list of matrix minerals considered during model calculations other than the precipitates in Table 2 is given in Table 3.

3.2.2. Adsorption and surface exchange

Surface complexation of sulphate, arsenate, arsenite, selenite and selenite to amorphous iron oxides, also called hydrous ferric oxides (HFO) was modelled using the Diffuse Layer/Surface Complexation Model (DL/SC) [35]. The thermodynamic data set used for As and Se is shown in Table 4. Dzombak and Morel [35] recommend using 600 m^2/g as a specific surface area and 0.2 mol active sites per mol of Fe as charge density for HFO. The magnitude of the adsorbing surface of HFO was calculated from the modelled amount of ferrihydrite ($Fe(OH)_3(a)$).

Surface exchange of arsenite and selenite with carbonate on calcite was modelled using exchange constants from Roman-Ross et al. [18] and empirical half-exchange reactions from Cowan et al.

Table 3
Minerals other than those listed in Table 2 which were allowed to precipitate during model calculations

Reaction	log *K*	Source
$Ca_{0.8}SiO_5H_{4.4} + 1.6H^+ = 0.8Ca^{2+} + H_4SiO_4 + H_2O$	11.03	[62]
$Ca_{1.1}SiO_7H_{7.8} + 2.2H^+ = 1.1Ca^{2+} + H_4SiO_4 + 3H_2O$	16.66	[62]
$Ca_{1.8}SiO_9H_{10.4} + 3.6H^+ = 1.8Ca^{2+} + H_4SiO_4 + 5H_2O$	32.41	[62]
$CaSO_4{\cdot}2H_2O = Ca^{2+} + SO_4^{2-} + 2H_2O$	−4.58	[21]
$Ca_6Al_2(OH)_{12}(SO_4)_3{\cdot}26H_2O + 12H^+ = 6Ca^{2+} + 2Al^{3+} + 3SO_4^{2-} + 38H_2O$	56.85	[63]
$Ca(OH)_2 + 2H^+ = Ca^{2+} + 2H_2O$	74.0928	[29]
$CaCO_3 = Ca^{2+} + CO_3^{2-}$	−8.48	[25]
$Fe(OH)_3\ (a)^a + 3H^+ = Fe^{3+} + 3H_2O$	4.891	[25]
$Fe(OH)_2 + 2H^+ = Fe^{2+} + 2H_2O$	13.49	[25]
$Al(OH)_3\ (a)^a + 3H^+ = Fe^{3+} + 3H_2O$	10.8	[25]
$Mg(OH)_2 + 2H^+ = Mg^{2+} + 2H_2O$	17.1	[29]

[a] (a) = amorphous.

Table 4
Thermodynamic data used for adsorption modelling

Reaction	log K_{int}	Source
As^{V}		
$-FeOH + AsO_4^{3-} + 3H^+ = -FeH_2AsO_4 + H_2O$	29.88	[64]
$-FeOH + AsO_4^{3-}\ 2H^+ = -FeHAsO_4^- + H_2O$	24.81	[64]
$-FeOH + AsO_4^{3-} + H^+ = -FeAsO_4^{2-} + H_2O$	18.10	[64]
As^{III}		
$-FeOH + AsO_3^{3-} + 3H^+ = -FeH_2AsO_3 + H_2O$	38.76	[64]
$-FeOH + AsO_3^{3-} + 2H + = -FeHAsO_3^- + H_2O$	31.87	[64]
Se^{VI}		
$-FeOH + SeO_4^{2-} + H^+ = -FeSeO_4 + H_2O$	7.73	[35]
$-FeOH + SeO_4^{2-} = -FeOHSeO_4^{2-}$	0.8	[35]
Se^{IV}		
$-FeOH + HSeO_3^- + H^+ = -FeSeO_3 + H_2O$	12.69	[35]
$-FeOH + HSeO_3^- = -FeOHSeO_3^{2-} + H^+$	5.17	[35]

Table 5
Surface exchange reaction constants for arsenite and selenite exchange with carbonate on calcite surfaces

Exchange reaction	log K	Source
$XCO_3 + H_3AsO_3^0 = H_2CO_3 + XHAsO_3$	1.274	[18]
Half-exchange reaction		
$CO_3^{2-} + 2X^+ = X_2CO_3$	12.5	[19]
$H^+ + CO_3^{2-} + X^+ = XHCO_3$	16.76	[19]
$SeO_3^{2-} + 2X^+ = S_2SeO_3$	16.70	[19]
$H^+ + SeO_3^{2-} + X^+ = XHSeO_3$	16.92	[19]

[19] (Table 5). Roman-Ross et al. [18] used a specific surface area of 0.2 m^2/g calcite and determined a maximum of 6 active sites/nm^2 for $H_3AsO_3^0$ adsorption, which leads to 0.02 mol active sites per mol calcite. The modelled amount of calcite was used as the adsorbing surface in case of selenite adsorption because Cowan et al. [19] did not relate the empirical constant with the amount of active sites.

Selenite adsorption on ettringite was approximated using a distribution ratio, $R_d = ([SeO_3^{2-}]_{adsorbed}/[SeO_3^{2-}]_{aq})S$, where $[SeO_3^{2-}]_{adsorbed}$ is the adsorbed Se^{IV} concentration in equilibrium with $[SeO_3^{2-}]_{aq}$ in solution and S is the ettringite concentration expressed as g/l for which the modelled amount of ettringite was used in this case. A value of $R_d = 0.18\ m^3/kg$ was taken from Baur and Johnson [12] who experimentally found a sorption maximum of 0.3 mol selenite per kg ettringite which corresponds to the maximum of 0.038 mol available sites per mol ettringite which was set in model calculations.

3.2.3. Solid solution formation

Solid solution formation was considered for $CaSO_4/Ca_3(AsO_4)_2$, $Ca(SeO_3,CO_3)$, $Ca(SeO_4,CO_3)$, $Ca(SO_4,SeO_4)\cdot 2H_2O$, and $Ca_6Al_2(SO_4,SeO_4)_3(OH)_{12}\cdot 26H_2O$. All solid solutions, except $Ca(SO_4,SeO_4)\cdot 2H_2O$, were considered ideal in this study due to lack of thermodynamic data to account for non-ideality. The activity coefficients of $CaSeO_4\cdot 2H_2O$ and $CaSO_4\cdot 2H_2O$ in the non-ideal $Ca(SO_4,SeO_4)\cdot 2H_2O$ solid solution, on the other hand, were calculated by Fernandez-Gonzalez et al. [15] using the Lippman model as described by Glynn [36]. A regular solid solution was considered by Fernandez-Gonzalez et al. [15] in which all Guggenheim parameters are set to 0 except the first one that was calculated to be $a_0 = 2.238$.

PHREEQC is not capable of calculating non-ideal solid solutions of more than two components, so it was not possible to calculate Se^{VI} concentrations in equilibrium with both the non-ideal $Ca(SO_4,SeO_4)\cdot 2H_2O$ solid solution and the ideal $Ca(SeO_4,CO_3)$ solid solution. Three consecutive model calculations were therefore executed in case of Se^{VI}:

- Considering precipitation only (Model 1).
- Considering the non-ideal $Ca(SO_4,SeO_4)\cdot 2H_2O$ solid solution combined with an ideal $Ca_6Al_2(SO_4,SeO_4)_3(OH)_{12}\cdot 26H_2O$ solid solution (Model 2).
- Considering ideal $Ca(SO_4,CO_3,SeO_4)$ and $Ca_6Al_2(SO_4,SeO_4)_3(OH)_{12}\cdot 26H_2O$ solid solution (Model 3).

4. Results and discussion

4.1. Total and leachable amounts

Table 6 shows the total content of elements in the sludge and the results of the EN 12457-2 test. The most abundant elements are Ca, S, As, Al, Se, Fe, Na and K. The total content and leachability of As and Se are high compared to other types of alkaline waste such as coal fly ash [6,37] or cement-stabilised wastes [38] and both As and Se leaching are above European standards for landfilling of hazardous waste (25 mg/kg and 7 mg/kg, respectively). The sludge also contain significant amounts of Pb, Zn, Cd and Cu but no leached concentrations of these elements were above European standards.

Based on the Eh–pH diagram of As [7], As is likely to occur predominantly in the pentavalent form at the measured Eh–pH values (Table 6) and from the Eh–pH diagram of Se, both Se^{VI} and Se^{IV} are expected, which is confirmed by the total speciation of As and Se in Table 6 and the pH-dependent redox speciation of As and Se of the second pH-dependent leaching test (Fig. 1). The carbonate content of the samples used for this test had increased to 0.29 mol/kg and the natural pH had decreased to 10.4 indicating that carbonation, the reaction with atmospheric CO_2, had occurred. This was taken into account when modelling pH-dependent speciation results but it was assumed that redox speciation of As and Se was not altered with respect to the first test given the slow kinetics of redox reactions of these elements in inorganic alkaline solid wastes [26,27].

4.2. Mineralogy

Fig. 2 shows the XRD diffractogram of the original and washed sample. Clearly, gypsum is the dominant mineral in the unwashed

Table 6
Characteristics of suspensions and total and leached (L/S = 10) amounts from the sludge sample

pH		11.1
Eh (mV)		410
Element	Total (mol/kg)	Leached[a] (mg/kg)
Ca	6.11	6935
As	0.899	38.03
As^{III}/As_{total} (%)	3.7	
Se	0.036	19.53
Se^{IV}/Se_{total} (%)	21.3	
Fe	0.248	<LOD[b]
Al	0.232	1.51
K	0.329	45.46
Na	0.471	2263
Mg	0.115	<LOD[b]
Cu	0.029	<LOD[b]
Zn	0.044	<LOD[b]
Cd	0.005	2.07
Sb	0.011	7.00
Pb	0.014	<LOD[b]
Ba	0.0006	<LOD[b]
SO_4^{2-}	4.16	1500
Si	0.089	<LOD[b]
CO_3^{2-}	0.17	NA[c]

[a] Average leached amounts of three replicates at the pH indicated.
[b] Limit of detection.
[c] Not available.

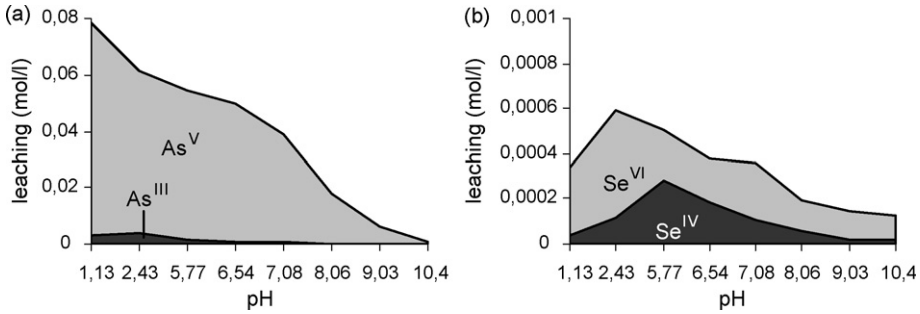

Fig. 1. Redox speciation of soluble (a) As and (b) Se in the second pH-dependent leaching test.

sample, which is not surprising given the high calcium and sulphur content (Table 6). After washing at L/S = 200, the gypsum peaks are significantly reduced and the minerals rauenthalite ($Ca_3(AsO_4)_2{\cdot}10H_2O$) and calcite can be discerned. The presence of calcite indicates that some carbonation of the alkaline material has occurred during storage, prior to sampling.

During SEM-EDS analysis, As was found to be scattered throughout the sample and large calcium arsenate crystals appeared to be scarce. Fig. 3a shows a notable exception of platy crystals of a calcium arsenate with a molar Ca:As:O ratio of 3:2:24. Given the fact that a large spot size had to be used to collect enough counts for EDS analysis, counts for lighter elements such as oxygen or carbon were probably also collected from the underlying supporting layer and the actual oxygen content of the mineral in Fig. 3a probably is lower because the most hydrated calcium arsenate known is phaunoxite ($Ca_3(AsO_4)_2{\cdot}11H_2O$, Ca:As:O = 3:2:19). The crystals in Fig. 3a are, however, most likely rauenthalite (Ca:As:O = 3:2:18) because the occurrence of large amounts of phaunouxite would lead to a distinct peak at $2\theta = 8.9^\circ$ in the XRD diffractogram and the dehydration of phaunoxite to rauenthalite at room temperature is a known reaction [39].

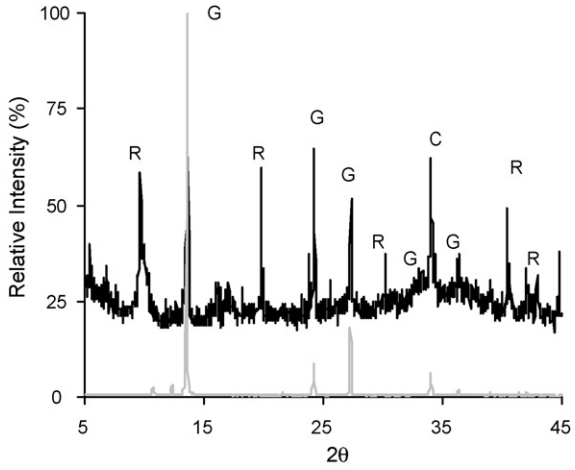

Fig. 2. XRD-diffractograms of original (gray) and washed samples (black). G = gypsum, R = rauenthalite, C = calcite.

The formation of hydrated calcium arsenates of the form $Ca_3(AsO_4)_2{\cdot}xH_2O$ has been reported in synthetic $CaO–As_2O_5$ mixtures with pH-values similar to the "natural" pH of the sludge sample (11.1) [31,33,40–45] but only Guerin et al. [40] found rauenthalite to precipitate whereas others found no higher hydration numbers than 4.25. It has been postulated that precipitation of calcium arsenates with high hydration numbers such as rauenthalite or phaunouxite indicates alkaline conditions with high levels of dissolved As and a low Ca availability [41]. Ca can indeed be expected to be less available in gypsum sludges compared to synthetic $CaO–As_2O_5$ mixtures due to the precipitation of gypsum and calcite. In conjunction with the high pH, the precipitation of rauenthalite is thus likely to occur.

In most cases, As was not found as large calcium arsenate crystals, but associated with gypsum crystals (Fig. 3b). This may either indicate a $CaSO_4/Ca_3(AsO_4)_2$ solid solution or small rauenthalite crystals precipitated on a larger gypsum phase, or both. No conclusion can be drawn based on these experimental results. However, it has been stated that arsenate interaction with gypsum mainly occurs through solid solution formation, especially at high pH [14]. Donahue and Hendry [26] also found that As was associated with gypsum minerals in their samples and suggested a solid solution of calcium arsenate in gypsum.

4.3. Mineral selection

Rauenthalite clearly dominates the arsenate mineralogy at the natural pH but does not necessarily do so at other pH values. In

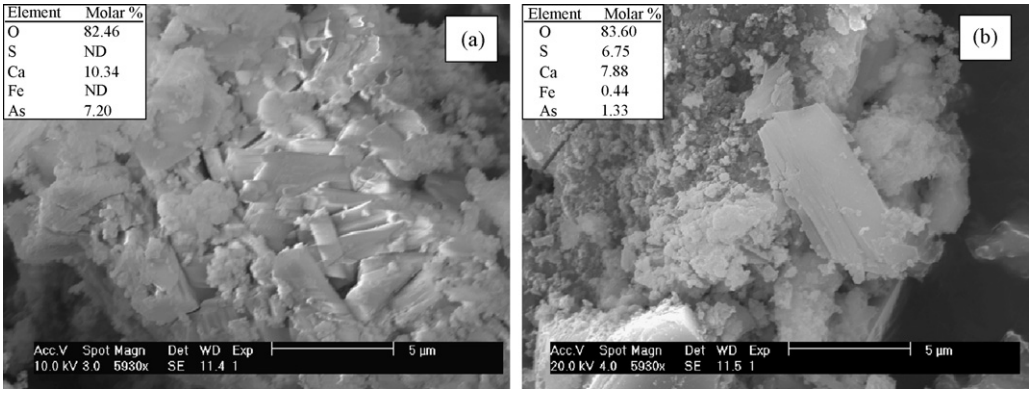

Fig. 3. SEM image and EDS spot analysis of (a) calcium arsenates, most likely rauenthalite (b) a gypsum crystal. ND: not detected.

Table 7
Recalculated solubility products of selected calcium arsenates from solubility data from [33]

Reactions	Association constant dataset, log K_{so}		
	None	Whiting [32]	Bothe and Brown [33]
$Ca_3(AsO_4)_2{\cdot}10H_2O = 3Ca^{2+} + 2AsO_4^{3-} + 10H_2O$	−20.19	−21.58	−21.46
$CaHAsO = Ca^{2+} + HAsO_4^{2-}$	−4.57	−4.84	−4.85

Explanation of the three different data sets, see paragraph on modelling in PHREEQC.

synthetic $CaO–As_2O_5$ mixtures, $CaHAsO_4{\cdot}H_2O$ is stable in the most acidic (pH < 6) conditions whereas $Ca_4(AsO_4)_2(OH)_2{\cdot}4H_2O$ precipitates in the most alkaline (pH > 12) mixtures [42–44]. However, in real systems where Ca is less available, the latter solid has not yet been detected. In As^V spiked cements that have a relatively high pH (>12.5), arsenate mineralogy is usually dominated by calcium arsenates with a lower Ca:As ratio than $Ca_4(AsO_4)_2(OH)_2{\cdot}4H_2O$ such as $Ca_5(AsO_4)_3OH$, $Ca_3(AsO_4)_2{\cdot}xH_2O$, $CaNaAsO_4{\cdot}7.5H_2O$ and $CaHAsO_4$ [11,45–48]. The Na content of the sludge is too low relative to the Ca and As content to allow significant $CaNaAsO_4{\cdot}7.5H_2O$ formation and $Ca_5(AsO_4)_3OH$ formation is inhibited in the presence of Mg ions [42,43]. Rauenthalite and $CaHAsO_4$ were therefore the only calcium arsenates considered for modelling and their solubility products were recalculated from solution compositions in equilibrium with calcium arsenates taken from Bothe and Brown [33] (Table 7). In case of rauenthalite, the solubility product was calculated from a solution composition in equilibrium with $Ca_3(AsO_4)_2{\cdot}4.5H_2O$ because no solution composition in equilibrium with rauenthalite was available in the literature but the solubility of the 4.5 hydrate is highly similar to that of rauenthalite [43].

Although no arsenite or selenium minerals could be detected, $CaHAsO_3$, $CaSeO_3{\cdot}H_2O$ and $CaSeO_4{\cdot}2H_2O$ were assumed to have precipitated because they are the most stable calcium arsenite, selenite, and selenate, respectively at ambient conditions [46,49–51].

4.4. Modelling results

4.4.1. Prevailing minerals

As can be seen in Fig. 4, the most important minerals at the unaltered pH are predicted to be gypsum, rauenthalite, calcite, ettringite and amorphous iron oxides. Ettringite was not detected during XRD analysis, probably due to peak overlap and the absence of a single intense peak, contrary to calcite. Amorphous compounds like HFO generally do not show peaks in an XRD diffractogram. Fig. 4 also shows that the present mineral selection leads to an accurate prediction of the leaching behaviour of Ca, the most important matrix element, up to pH 12.5.

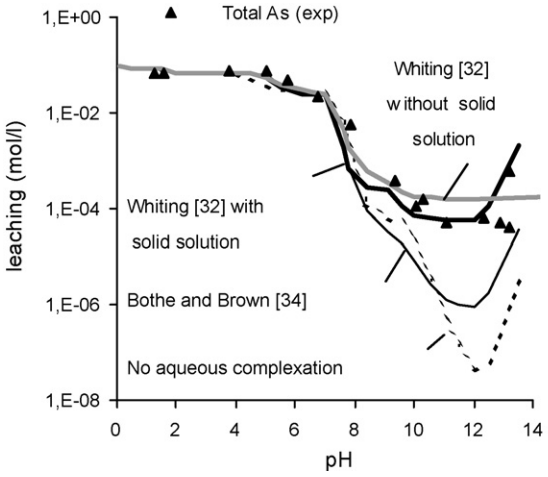

Fig. 5. Modelling of pH-dependent total As leaching considering aqueous complexation constants for $CaAsO_4^-$, $CaHAsO_4^0$, and $CaH_2AsO_4^+$ of Whiting [32], Bothe and Brown [33] and none at all. In case of the Whiting dataset, modelling results are depicted both with and without considering solid solutions. In other cases, no solid solutions were considered.

4.4.2. Arsenic

Fig. 5 shows the result of As leaching modelling. Using the dataset without aqueous Ca–As^V complexes leads to an underestimation of four orders of magnitude, which suggests that such complexes do exist. Raposo et al. [31] found no evidence of the formation of such complexes when performing an acid titration of a 1 mM AsO_4^{3-} solution with or without the addition of 1 mM Ca^{2+} but these authors only titrated up to pH 10, whereas the difference between experimental and modelled results when no aqueous complexes are considered, is most pronounced at pH > 10 (Fig. 5).

When the dataset with association constants calculated by Bothe and Brown [33] for $CaAsO_4^-$, $CaHAsO_4^0$, and $CaH_2AsO_4^+$ are used, As-minerals at alkaline pH are predicted to be oversaturated by two orders of magnitude. Donahue and Hendry [26] also found that the implementation of aqueous complexation constants of Bothe and Brown [33] leads to prediction of oversaturation of calcium arsenates. In this case, using the dataset of Whiting [32] gives the best fit with experimental results.

Applying solid solution formation with gypsum, as suggested by Donahue and Hendry [26] and Fernandez-Martinez et al. [14], further improved prediction of the experimental results (Fig. 5).

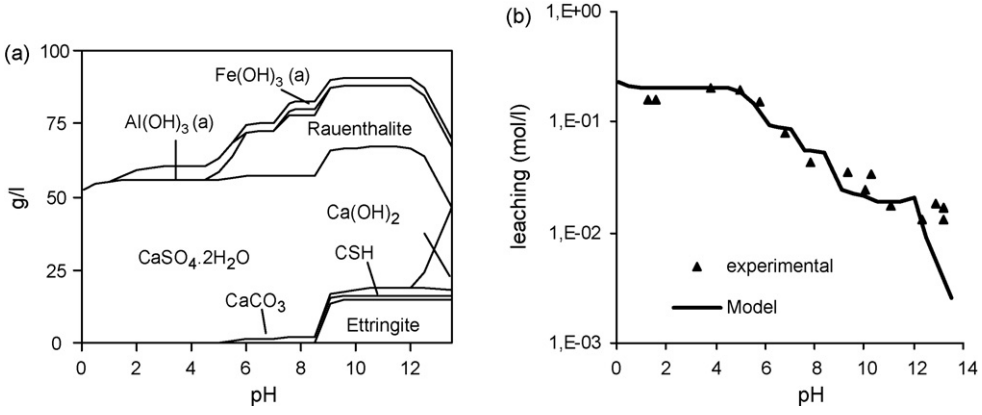

Fig. 4. (a) Modelled pH-dependent presence of the most important minerals in the sludge expressed as g/l (L/S = 10) and (b) the modelled pH-dependent Ca leaching in the sludge sample.

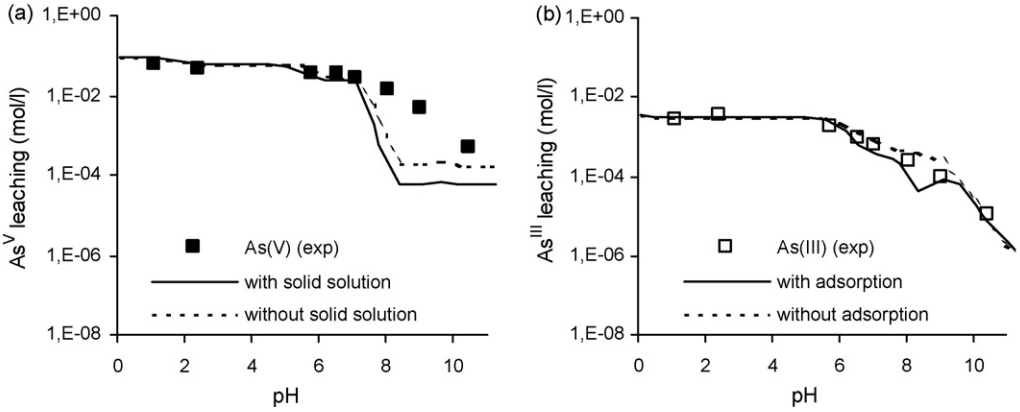

Fig. 6. Modelling of As^V and As^{III} leaching in the second pH-dependent leaching test with and without considering solid solutions.

The incorporation of As^V in ettringite, which is a likely mechanism in alkaline matrices [13], could however not be taken into account, because the solubility of the arsenate analogue of ettringite has not yet been determined. Adsorption to iron oxides, when applied, did not alter results significantly.

Modelling of pH-dependent As^V and As^{III} leaching as a function of pH was executed on speciation results from the second pH-dependent test as shown in Fig. 6. In case of As^V, the dataset of Whiting [32] was used because it gave the best results when modelling total As leaching. Modelling with and without considering solid solution are depicted but a poor fit with experimental results is observed in both cases at pH > 7. The fit was even poorer when the $CaSO_4/Ca_3(AsO_4)_2$ solid solution was taken into account. Fernandez-Martinez et al. [14] found that the incorporation of arsenate in gypsum significantly distorts its crystal structure, which suggests that the best way to describe the interaction of arsenate with gypsum would be through non-ideal solid solution formation. Why including solid solution worsens the fit for As^V, whereas it improves the fit for total As (Fig. 5) could not be explained but it appears that solid solution formation as a leaching controlling mechanism is much less important compared to calcium arsenate precipitation. Calcium arsenates are sparingly soluble compared to other calcium metalates in alkaline matrices and, although gypsum is an exceptionally abundant mineral in this sample, it is much more soluble than calcium arsenates and will therefore not incorporate much arsenate.

A similar observation can be made in Fig. 6 where the As^{III} leaching is very well predicted but consideration of As^{III} adsorption on calcite does not significantly improve model predictions. Calcium arsenites are quite stable in an alkaline environment [51] but the limited differences between the two models (with/without calcite adsorption) can also be ascribed to the relatively low calcite (Fig. 4) and As^{III} (Table 6) content.

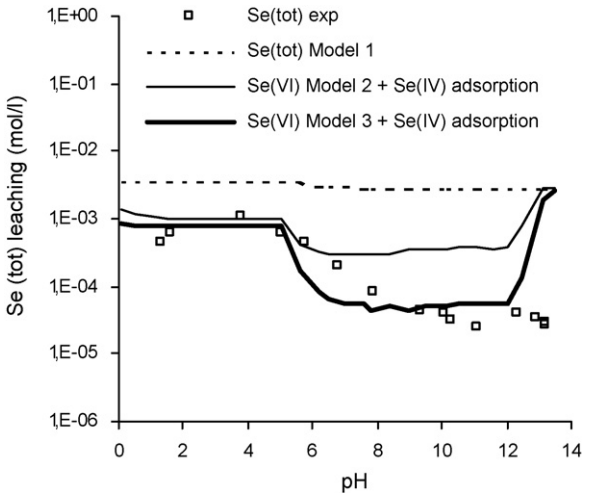

Fig. 7. Modelling of pH-dependent total Se leaching of the first test. Model 1: precipitation only, Model 2 for Se^{VI} and surface adsorption of selenite on calcite and ettringite, Model 3 for Se^{VI} and surface adsorption of selenite on calcite and ettringite.

4.4.3. Selenium

Metal selenites and selenates are relatively soluble compared to other metal–oxyanion compounds and are thus more likely to be

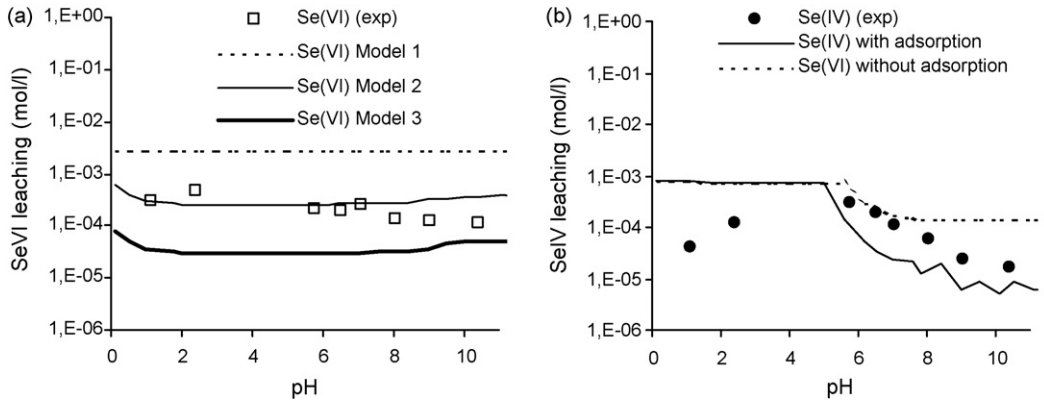

Fig. 8. Modelling of Se^{VI} and Se^{IV} leaching in the second pH-dependent leaching test.

controlled by processes other than precipitation, such as adsorption and solid solution formation [12]. This is evident from Fig. 7, showing the modelled leaching behaviour of total Se in the first pH-dependent leaching test. The three solid solution models for Se^{VI} as mentioned in the previous section were applied together with or without Se^{IV} adsorption to calcite and ettringite. Clearly, the fit of modelled results is less satisfactory compared to that obtained for As which can for a large part be attributed to the lack of up-to-date thermodynamic data of Se [52].

When only precipitation was considered (Model I for Se^{VI}), Se^{VI} was predicted to be in equilibrium with $BaSeO_4$ rather than $CaSeO_4{\cdot}2H_2O$, illustrating the high solubility of the latter solid even in this calcium-rich matrix. The solubility of $CaSeO_4{\cdot}2H_2O$ is reduced significantly by forming a solid solution with gypsum (Model 2 for Se^{VI}) but this is probably not the only mechanism that controls Se^{VI} leaching, especially at alkaline pH. As is suggested by Fig. 8, interactions with calcite further lower Se^{VI} solubility at pH > 5.5 whereas solid solution formation of selenate with ettringite was quantitatively much less important (Model 2 for Se^{VI}). Baur and Johnson [12] found a relatively low affinity of selenate for ettringite although solid solution formation is a plausible mechanism. The interaction with calcite, as suggested by Staudt et al. [16], is in this case much more important. However, the approach used in this study, where calcium selenate forms an ideal solid solution with calcite, probably is an approximation that can explain the lack of fit with experimental results since Fernandez-Martinez et al. [14] found that replacement of trigonal CO_3^{2-} ions by tetrahedral SeO_4^{2-} oxyanions significantly deforms the calcite crystal structure and Staudt et al. [16] found that selenate partitioning at calcite surfaces is dependent on the pathway by which this process proceeds.

The solubility of $CaSe^{IV}O_3{\cdot}H_2O$, on the other hand, is much lower relative to that of $CaSe^{VI}O_4{\cdot}2H_2O$ but Fig. 8 suggests that Se^{IV} is not in equilibrium with $CaSeO_3{\cdot}H_2O$ at pH > 7.5. Ca^{2+} and CO_3^{2-}, rather than H^+ and ^-OH, are the potential determining ions for calcite surfaces [53], which enable this mineral to sorb oxyanions at much higher pH values compared to iron oxides. Cheng et al. [20] found that selenite is selectively adsorbed by exchange with CO_3^{2-} on calcite surfaces by forming a two-dimensional solid solution of the form $Ca(SeO_3)_x(CO_3)_{1-x}$. Moreover, ettringite has reactive $\equiv Ca{-}OH_2$ and $\equiv Ca_2{-}OH$ surface sites that can sorb anions at high pH [13] and has also proven to be an effective adsorbent for selenite [12]. The fit with experimental results is, however, not perfect. The model of Cowan et al. [19], which is used for the adsorption of Se^{IV} on calcite is based on empirically defined half reactions and modelling adsorption by application of a distribution ratio, as was done in case of adsorption of selenite to ettringite, does not incorporate competitive effects of other sorbing anions. Again, lack of fundamental models for adsorption with minerals occurring in alkaline residues hampers efficient modelling of the leaching behaviour but these results suggest that the presence of ettringite significantly influences the leaching of Se^{IV} and that calcite is an important sink for both selenite and selenate in the investigated matrix. The presence of calcite is especially of interest with respect to leaching of As^{III}, Se^{VI} and Se^{IV} at alkaline pH when considering carbonation, which greatly affects oxyanion leaching behaviour in alkaline matrices (e.g. [54]) because contrary to As^V, carbonation will not necessarily invoke higher As^{III}, Se^{VI} or Se^{IV} leaching values.

5. Conclusion

The leaching behaviour of As and Se in alkaline gypsum matrices is controlled by precipitation of calcium metalates and most likely also by adsorption and solid solution with abundant minerals. The leaching behaviour of arsenic was reasonably well predicted when precipitation of rauenthalite was considered as a controlling mechanism but only if a consistent dataset was used that contained association constants of soluble $Ca{-}As^V$ aqueous complexes from Whiting [32]. Indications have been found that $CaSO_4/Ca_3(AsO_4)_2$ solid solution formation and arsenite adsorption to calcite further decrease As^V and As^{III} leachability below calcium metalate saturation but the effect of these mechanisms is relatively limited due to the already low solubility of calcium arsenate and arsenite in alkaline matrices.

In case of Se, lack of thermodynamic data hampers efficient modelling but it appears that the relatively high solubility of selenium precipitates enables adsorption and solid solution to gain importance as controlling mechanisms relative to arsenic. It is suggested that the development of an efficient model for oxyanion interaction with matrix minerals of alkaline matrices can further improve model efforts of selenium leaching behaviour since calcite may be an important sink for both selenite and selenate and ettringite for selenite in both the investigated matrix and other alkaline matrices.

Acknowledgments

The authors would like to thank Dr. Annette Johnson (EAWAG, Switzerland) for invaluable guidance and the use of HG-ICP-OES and Hermann Mönch (EAWAG, Switzerland) for technical guidance with HG-ICP-OES. The departments of metallurgy/material sciences and geology at KULeuven, Belgium are thanked for the use of SEM-EDS and XRD, respectively.

References

[1] J.A. Meima, R.N.J. Comans, Geochemical modelling of weathering reactions in municipal solid waste incinerator bottom ash, Environ. Sci. Technol. 31 (1997) 1269–1276.
[2] C.E. Halim, S.A. Short, J.A. Scott, R. Amal, G. Low, Modelling the leaching of Pb, Cd, As, and Cr from cementituous waste using PHREEQC, J. Hazard. Mater. 125 (2005) 45–61.
[3] W.J.J. Huijgen, R.N.J. Comans, Carbonation of steel slag for CO_2 sequestration: leaching of products and reaction mechanisms, Environ. Sci. Technol. 40 (2006) 2790–2796.
[4] A.M. Fällman, J. Hartlén, Leaching of slags and ashes—controlling factors in field experiments versus in laboratory tests, in: J.J.J.M. Goumans, H.A. van der Sloot, T.G. Aalbers (Eds.), Studies in Environmental Science 60, Environmental Aspects of Construction with Waste Materials, Elsevier, Amsterdam, 1994, pp. 39–54.
[5] IAWG, Municipal Solid Waste Incinerator Residues. Studies in Environmental Science 67, Elsevier, Amsterdam, 1997.
[6] USGS, Historical Statistics for Mineral and Material Commodities in the United States. Open-File Report 01-006, version 9.1, US Geological Survey, 2005.
[7] C.F. Baes, R.E. Mesmer, The Hydrolysis of Cations, Wiley, New York, 1976.
[8] ATSDR, Toxicological Profile for Arsenic. PB/2000/108021, US Department of Health and Human Services, 2000.
[9] S.B. Goldhaber, Trace element risk assessment: essentiality vs. toxicity, Regul. Toxicol. Pharm. 38 (2003) 232–242.
[10] T. Van Gerven, D. Geysen, L. Stoffels, M. Jaspers, G. Wauters, C. Vandecasteele, Management of incinerator Residues in Flanders (Belgium) and neighbouring countries. A Comparison, Waste Manage. 25 (2005) 75–87.
[11] C. Vandecasteele, V. Dutré, D. Geysen, G. G. Wauters, Solidification/stabilization of arsenic bearing fly ash from the metallurgical industry. Immobilization mechanism of arsenic, Waste Manage. 22 (2002) 143–146.
[12] I. Baur, C.A. Johnson, Sorption of selenite and selenate to cement minerals, Environ. Sci. Technol. 37 (2003) 3442–3447.
[13] S.C.B. Myneni, S.J. Traina, T.J. Logan, G.A. Waychunas, Oxyanion behavior in alkaline environments: sorption and desorption of arsenate in ettringite, Environ. Sci. Technol. 31 (1997) 1761–1768.
[14] A. Fernández-Martínez, G. Román-Ross, G.J. Cuello, X. Turillas, L. Charlet, M.R. Johnson, F. Bardelli, Arsenic uptake by gypsum and calcite: Modelling and probing by neutron X-scattering, Physica B 385/386 (2006) 935–937.
[15] A. Fernandez-Gonzalez, A. Andara, J. Alia, M. Prieto, Miscibility in the $CaSO_4{\cdot}2H_2O{-}CaSeO_4{\cdot}2H_2O$ system: implications for the crystallisation and dehydration behaviour, Chem. Geol. 225 (2006) 256–265.
[16] W.F. Staudt, R.J. Reeder, M.A.A. Schoonen, Surface structural controls on compositional zoning of SO_4^{2-} and SeO_4^{2-} in synthetic single crystals, Geochim. Cosmochim. Acta 58 (1994) 2087–2098.
[17] L. Cheng, P. Fenter, N.C. Sturchio, Z. Zhong, M.J. Bedzyk, X-ray standing wave study of arsenite incorporation at the calcite surface, Geochim. Cosmochim. Acta 63 (1999), 3253-3157.

[18] G. Roman-Ross, G.J. Cuello, X. Turillas, A. Fernandez-Martinez, L. Charlet, Arsenite sorption and co-precipitation with calcite, Chem. Geol. 233 (2006) 328–336.
[19] C.E. Cowan, J.M. Zachara, C.T. Resch, Solution ion effects on the surface exchange of selenite on calcite, Geochim. Cosmochim. Acta 54 (1990) 2223–2234.
[20] L. Cheng, P.F. Lyman, N.C. Sturchio, M.J. Bedzyk, X-ray standing wave investigation of the surface structure of selenite anions adsorbed on calcite, Surf. Sci. 382 (1997) L690–L695.
[21] M. Ochs, B. Lothenbach, E. Giffaut, Uptake of oxo-anions by cements through solid-solution formation: experimental evidence and modelling, Radiochim. Acta 90 (2002) 639–646.
[22] US-EPA, Identification and Description of Mineral Processing Sectors and Waste Streams, RCRA Docket No. F-96-PH4A-S0001, U.S. Environmental Protection Agency, 1995.
[23] M. Leist, R.J. Casey, D. Caridi, The management of arsenic wastes: problems and prospects, J. Hazard. Mater. B76 (2000) 125–138.
[24] M.W. George, Selenium and tellurium, in: Minerals Yearbook. Metals and Minerals, vol, I, U.S. Geological Survey, 2006.
[25] D.L. Parkhurst, C.A.J. Appelo, PHREEQC (Version 2.12.5.669)—A Computer Program for Speciation, Batch-reaction, One-dimensional Transport, and Inverse Geochemical Calculations, U.S. Geological Survey, 2005.
[26] R. Donahue, M.J. Hendry, Geochemistry of arsenic in uranium mine mill tailings, Saskatchewan, Canada, Appl. Geochem. 18 (2003) 1733–1750.
[27] I. Bonhoure, I. Baur, E. Wieland, C.A. Johnson, A.M. Scheidegger, Uptake of Se(IV/VI) oxyanions by hardened cement paste and cement minerals: an X-ray absorption spectroscopy study, Cement Concrete Res. 36 (2006) 91–98.
[28] N.J. Welham, K.A. Malatt, S. Vukevic, The stability of iron phases presently used for disposal from metallurgical systems—a review, Miner. Eng. 13 (2000) 911–931.
[29] US-EPA, Minteqa2/prodefa2, A Geochemical Assessment Model for Enivronmental Systems: User Manual Supplement for Version 4.0, National Exposure Research Laboratory, Ecosystems Research division, Athens, GA, 1999.
[30] T. Nishimura, R.G. Robins, A Re-Evaluation of the Solubility and Stability regions of calcium arsenites and calcium arsenates in aqueous solution at 25 °C, Miner. Process. Extr. Metall. Rev. 18 (1998) 283–308.
[31] J.C. Raposo, O. Zuloaga, M.A. Olazabal, J.M. Madariaga, Study of the precipitation equilibria of arsenate anion with calcium and magnesium in sodium perchlorate at 25 °C, Appl. Geochem. 19 (2004) 855–862.
[32] K.S. Whiting, The Thermodynamics and Geochemistry of As with the Application to Subsurface Waters at the Sharon Steel Superfund Site Midvale, Utah, MSc, Colorado School of Mines, 1992.
[33] J.V. Bothe, P.W. Brown, The stabilities of calcium arsenates at 23 ± 1 °C, J. Hazard. Mater. B69 (1999) 197–207.
[34] D. Nordstrom, D. Archer, Arsenic thermodynamic data and environmental geochemistry—an evaluation of thermodynamic data for modelling the aqueous environmental geochemistry of arsenic, in: A.H. Welch, K.G. Stollenwerk (Eds.), Arsenic in Ground Water: Geochemistry and Occurrence, Kluwer Academic Publishers, Dordrecht, 1999, pp. 1–26.
[35] D.A. Dzombak, F.M.M. Morel, Surface Complexation Modelling: Hydrous Ferric Oxide, John Wiley and Sons, New York, 1990.
[36] P.D. Glynn, Modelling solid-solution reactions in low temperature aqueous systems, in: D.C. Melchior, R.L. Basset (Eds.), Modelling in Aqueous Systems: II, ACS Symposium Series, 416, 1990, pp. 74–86.
[37] I. Lecuyer, S. Bicocchi, P. Ausset, R. Lefevre, Physico-chemical characterisation and leaching of desulfurization coal fly ash, Waste Manage. Res. 14 (1996) 15–28.
[38] J.E. Aubert, B. Husson, N. Sarramone, Utilization of municipal solid waste incineration (MSWI) fly ash in blended cement. Part 1. Processing and characterization of MSWI fly ash, J. Hazard. Mater. 136 (2006) 624–631.
[39] M. Catti, G. Ivaldi, On the topotactic dehydratation $Ca_3(AsO_4)_2{\cdot}11H_2O$ (phaunouxite) → $Ca_3(AsO_4)_2{\cdot}10H_2O$ (rauenthalite), and the structures of both minerals, Acta Crystallogr. B39 (1983) 4–10.
[40] H. Guerin, Sur Les Arseniates Alcalino-Terreux; Etude Du Systeme As_2O_5–$Ca(OH)_2$, Ann. Chim. 16 (1941) 101–153.
[41] M.C.F. Magalhaes, Arsenic—An environmental problem limited by solubility, Pure Appl. Chem. 74 (2002) 1843–1850.
[42] J.V. Bothe, P.W. Brown, Arsenic immobilisation by calcium arsenate formation, Environ. Sci. Technol. 33 (1999) 3806–3811.
[43] J.V. Bothe, P.W. Brown, CaO–As_2O_5–H_2O system at 23° ± 1 °C, J. Am. Ceram. Soc. 85 (2002) 221–224.
[44] Y.N. Zhu, X.H. Zhang, Q.L. Xie, D.Q. Wang, G.W. Cheng, Solubility and stability of calcium arsenates at 25 °C, Water Air Soil Pollut. 169 (2006) 221–238.
[45] H. Akhter, F.K. Cartledge, A. Roy, M.E. Tittlebaum, Solidification/stabilization of arsenic salts: effects of long cure times, J. Hazard. Mater. 52 (1997) 247–264.
[46] V. Dutré, C. Vandecasteele, Immobilization mechanism of arsenic in waste solidified using cement and lime, Environ. Sci. Technol. 32 (1998) 2782–2787.
[47] M.Y.A. Mollah, F. Lu, D.L. Cocke, An X-ray diffraction (XRD) and Fourier transform infrared spectroscopic (FT-IR) characterization of the speciation of arsenic(V) in Portland cement type-V, Sci. Total Environ. 224 (1998) 57–68.
[48] C.Y. Jing, G.P. Korfiatis, X.G. Meng, Immobilization mechanisms of arsenate in iron hydroxide sludge stabilized with cement, Environ. Sci. Technol. 37 (2003) 5050–5056.
[49] S. Sharmasarkar, K.J. Reddy, G.F. Vance, Preliminary quantification of metal selenite solubility in aqueous solutions, Chem. Geol. 132 (1996) 165–170.
[50] J.Q. Dumm, P.W. Brown, Phase formation in the system CaO–SeO_2–H_2O, J. Am. Ceram. Soc. 80 (1997) 2488–2494.
[51] S.A. Stronach, N.L. Walker, D.E. Macphee, F.P. Glasser, Reactions between cement and As(III) oxide: the system CaO–SiO_2–As_2O_3–H_2O at 25 °C, Waste Manage. 17 (1997) 9–13.
[52] F. Séby, M. Potin-Gautier, E. Giffaut, G. Borge, O.F.X. Donard, A critical review of thermodynamic data for selenium species at 25 °C, Chem. Geol. 171 (2001) 173–194.
[53] S.L.S. Stipp, Toward a conceptual model of the calcite surface: hydration, hydrolysis, and surface potential, Geochim. Cosmochim. Acta 63 (1999) 3121–3131.
[54] G. Cornelis, T. Van Gerven, C. Vandecasteele, Antimony leaching from uncarbonated and carbonated MSWI bottom ash, J. Hazard. Mater. A137 (2006) 1284–1292.
[55] M.A. Elrashidi, D.C. Adriano, S.M. Workman, W.L. Lindsay, Chemical equilibria of selenium in soils: a theoretical development, Soil Sci. 144 (1987) 141–152.
[56] R.P. Parker, K.R. Tice, D.N. Thomason, Effects of ion pairing with calcium and magnesium on selenate availability to higher plants, Environ. Toxicol. Chem. 16 (1997) 565–571.
[57] C.W. Liu, T.N. Narasimhan, Modelling of selenium transport at the Kesterson reservoir, California, USA, J. Contam. Hydrol. 15 (1994) 345–366.
[58] R.G. Robins, The Stability and Solubility of Ferric Arsenate: An Update, D.R. Gaskell (Ed.), Proceedings of the EPD Congress '90, Anaheim, February 19–22, 1994, pp. 93–104.
[59] S. Sharmasarkar, G.F. Vance, Soil and plant selenium at a reclaimed uranium mine, J. Environ. Qual. 31 (2002) 1516–1521.
[60] M.E. Essington, Estimation of the standard free energy of formation of metal arsenates, selenates and selenites, Soil Sci. Soc. Am. J. 52 (1988) 1574–1579.
[61] M. Duc, G. Lefèvre, M. Fédoroff, Sorption of selenite ions on hematite, J. Colloid Interface Sci. 298 (2006) 556–563.
[62] Hatches. The Harwell/Nirex Thermodynamic Database for Chemical Equilibrium Studies, version 13, Nuclear Energy Agency, 2000.
[63] R.B. Perkins, C.D. Palmer, Solubility of ettringite ($Ca_6[Al(OH)_6]_2(SO4)_3{\cdot}26H_2O$) at 5–75 degrees C, Geochim. Cosmochim. Acta 63 (1999) 1969–1980.
[64] S. Dixit, J.G. Hering, Comparison of arsenic(V) and arsenic(III) sorption onto iron oxide minerals: implications for arsenic mobility, Environ. Sci. Technol. 37 (2003) 4182–4189.